Phonons and electron-phonon interaction at the Sb(111) surface

Davide Campi,[1] Marco Bernasconi,[1] and Giorgio Benedek[1,2,*]

[1]*Dipartimento di Scienza dei Materiali, Università di Milano-Bicocca, Via R. Cozzi 53, I-20125 Milano, Italy*

[2]*Donostia International Physics Center (DIPC), P.M. de Lardizabal 4, 20018 San Sebastián/Donostia, Spain*

(Received 10 May 2012; published 20 August 2012)

The bulk and surface dynamics of Sb(111) and the corresponding electron-phonon interaction have been calculated by density functional perturbation theory. The surface phonon bands reveal features related to a remarkable stiffening of the surface bilayer with respect to the bulk ones. The main contribution to electron-phonon interaction involves transitions between surface and bulk states, mostly driven by bulk phonons, and is found to be in good agreement with the value derived from spin angle-resolved photoemission spectroscopy.

DOI: 10.1103/PhysRevB.86.075446 PACS number(s): 63.22.−m, 68.35.Ja, 63.20.dk

I. INTRODUCTION

Antimony has recently attracted renewed interest because it is present in several compounds belonging to the newly discovered class of topological insulators. These compounds are insulators in the bulk, but display metallic surface states whose properties can be inferred on the basis of the topology of the bulk electronic bands. Antimony, although it is a bulk semimetal, shares the same topological order of the 3D topological insulator $Bi_{1-x}Sb_x$, which gives rise to the two topologically protected spin-polarized metallic surface states detected by spin angle-resolved photoemission spectroscopy (ARPES).[1,2] While the electronic surface states of antimony have been intensively studied both experimentally and theoretically, little is known about the surface phonons of Sb and more generally, about the coupling between surface topologically protected states and phonons. ARPES measurements[3] of the linewidth of Sb(111) electronic surface states suggest that such states mostly couple with bulk phonons. This issue, as well as recent measurements of Bi(111) surface phonon dispersion curves with He atom scattering (HAS),[4] has motivated the present theoretical study of Sb(111) surface dynamics and electron-phonon (el-ph) interaction based on density-functional perturbation theory (DFPT). This work also aims at providing useful reference data for further studies of surface phonons in Sb-containing topological insulators such as Sb_2Te_3.

II. COMPUTATIONAL DETAILS AND BULK PHONON CALCULATIONS

The dynamical properties of the Sb(111) surface were studied by means of DFPT[5] as implemented in the QUANTUM-ESPRESSO package.[6] A norm-conserving pseudopotential with five valence electrons and the Perdew-Burke-Ernzerhof (PBE) approximation[7] for the exchange-correlation energy functional were used. Spin-orbit (SO) effects were treated self-consistently with fully relativistic pseudopotentials and the formalism for noncollinear spin magnetization.[8] The Kohn-Sham orbitals were expanded in plane waves up to an energy cutoff of 45 Ry. A Gaussian smearing of 0.01 Ry was introduced in the occupation of states to deal with the metallic character of Sb.

Antimony crystallizes in the A7 structure ($R\bar{3}m$ space group) that can be described by a rhombohedral unit cell with two atoms or by a conventional hexagonal cell with six atoms stacked in the ABCABC sequence.[9] The structure (see Fig. 1) consists of buckled bilayers perpendicular to the [111] direction, with strong intrabilayer bonds 2.9 Å long and weaker interbilayer bonds 3.4 Å long, similar in nature to the weak bonds in phase-change material GeTe and GeSbTe alloys.[10]

We optimized the bulk geometry by integrating the Brillouin zone (BZ) over a $12 \times 12 \times 12$ Monkhorst-Pack mesh.[11] The resulting equilibrium structural parameters are $a = 4.558$ Å, $\alpha = 57.26^\circ$, and $z = 0.2338$ without SO interaction, and $a = 4.555$ Å, $\alpha = 57.36^\circ$, and $z = 0.2341$ including SO coupling, to be compared with the experimental value of $a = 4.507$ Å, $\alpha = 57.11^\circ$, and $z = 0.2335$,[9] where the z parameter indicates the position of Sb atoms on sites $\pm(z,z,z)$ in the Wyckoff notation. These results are in agreement with previous *ab initio* calculations.[12]

The Fourier transform of the dynamical matrices on a discrete uniform mesh in the BZ provides the real-space interatomic force constants from which the phonon dispersion relations are calculated. The phonon dispersion curves for bulk Sb, calculated along the high-symmetry directions of the BZ with and without SO interaction, are displayed in Fig. 2 and compared with the inelastic neutron-scattering data.[13]

The results are similar to previous phonon calculations with the localized density approximation (LDA) functional.[14,15] Both calculations reproduce reasonably well the acoustic branches whereas the calculated optical branches are somewhat softer than the experimental ones, especially the TO modes at the Γ and X points where they are about 7% off. The effect of SO coupling appears to be rather small. These misfits are larger than usual for DFT calculations and are possibly due to well-known difficulties of generalized gradient approximation (GGA) functionals in describing weak bondings like the interaction between adjacent bilayers. The inclusion of an empirical van der Waals (vdW) correction according to Grimme *et al.*[16] yields a contraction of 4% of the equilibrium atomic volume with respect to that calculated with the PBE functional, slightly improving the agreement with experiments in the acoustic region but further worsening the description of the optical branches. The fact that a density increase yields a softening (a negative Grüneisen constant) of the optical phonons was observed in Raman spectra of Sb under pressure.[12] Even larger misfits with experiments were found with other functionals such as that of

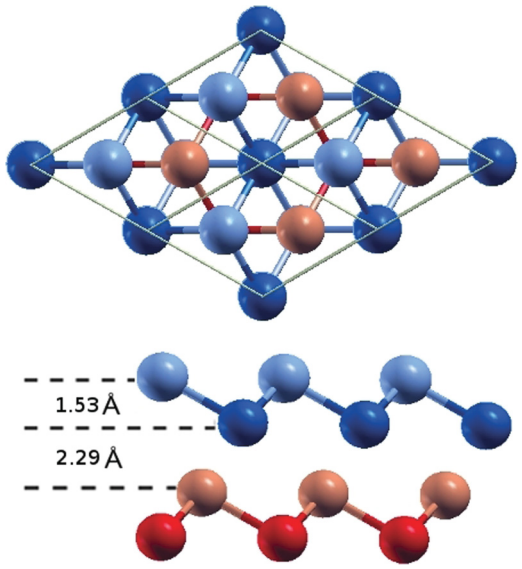

FIG. 1. (Color online) Top and side view of Sb(111). The distances in angstroms refer to interplanar distances along the [111] direction.

Becke-Lee-Yang-Parr[17,18] plus the semiempirical vdW correction. The PBE functional without vdW correction was therefore adopted for the calculations of surface dynamics and electron-phonon interaction. The nonoptimal description of the optical region is however sufficient to unravel the salient features of the surface phonon spectrum and the corresponding electron-phonon coupling.

The surface was modeled by a slab geometry with a single atom per layer and a variable number of layers (see Fig. 1). Twelve and 24 layers were used for calculations without SO coupling, while for calculations including SO coupling only the 12-layer slab was used. The slabs were separated by a vacuum 12 Å wide. The hexagonal surface Brillouin zone (SBZ) was sampled over a $8 \times 8 \times 1$ Monkhorst-Pack grid. Atomic positions were relaxed until forces became lower than 0.1 mRy/bohr. The SO interaction has a negligible effect on surface structure. After relaxation the outermost intrabilayer separation decreases by 0.3% while the distance between the second and third layer (interbilayer distortion) increases by 2%. The dynamical matrix was calculated on a $8 \times 8 \times 1$ mesh of q points in the SBZ.

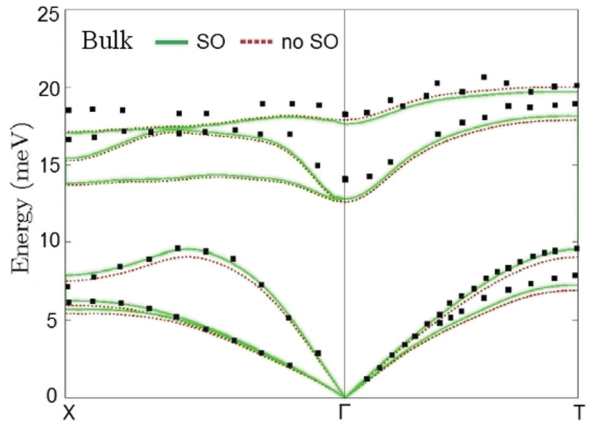

FIG. 2. (Color online) Bulk phonon dispersion of Sb, with SO coupling (solid green line) and without (dashed red line). The points are experimental neutron-scattering data from Ref. 13.

III. SURFACE ELECTRONIC PROPERTIES

The (111) surface of Sb displays two bands of topologically nontrivial surface states identified experimentally in Ref. 2. The electronic band structure of Sb(111) along the path K-Γ-M of the surface BZ is shown in Fig. 3 by neglecting or including SO coupling. The surface states arise at 235 meV below the Fermi level at Γ, where they are degenerate. In the presence of SO interaction the two surface bands are split out of Γ and form a Dirac cone structure; the upper and the lower surface states merge then with the conductionlike and valencelike bands, respectively, losing their surface character. Our results are similar to those of previous DFT work[19] and are in good agreement with ARPES data.[1,3,19]

The calculated expectation values of the spin operator on the two surface bands show a rather complex behavior: along the Γ-M direction the spin polarization vector is almost completely contained in the surface plane, similarly to results found experimentally.[1] The magnitude of spin projection is

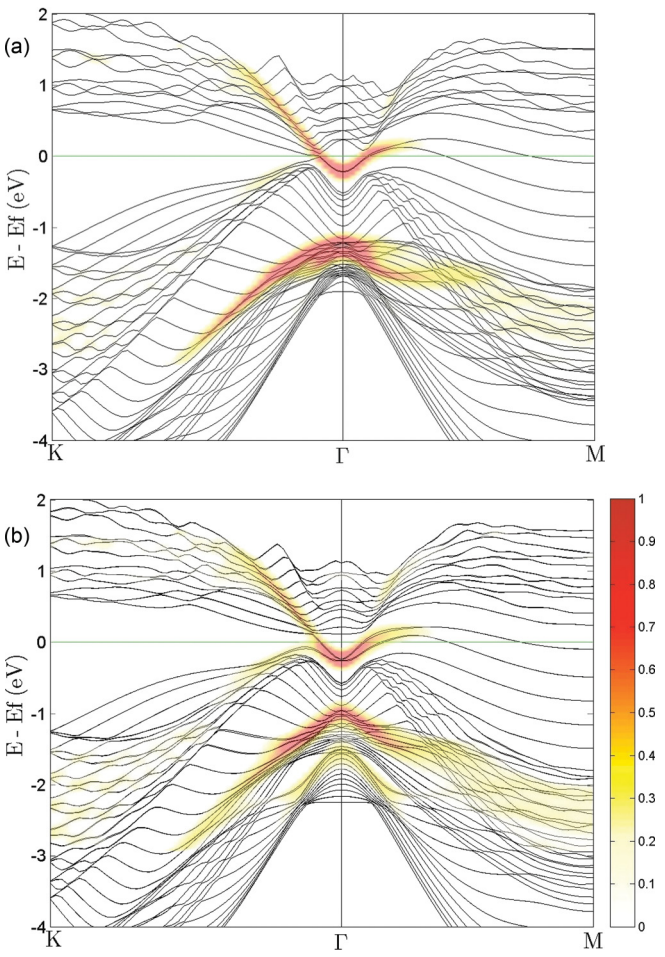

FIG. 3. (Color online) Electronic states of the Sb(111) slab without (a) and with (b) SO coupling. The gray scale indicates an increasing degree of localization of the electronic state on the surface atomic layer. The zero of the energy scale is the Fermi level.

about 90%, a value significantly higher than that computed for Bi-based topological insulators.[20] This can be understood by considering the smaller SO coupling of Sb with respect to Bi. Along Γ-K the spin polarization vector quickly develops an appreciable out-of-plane polarization, an effect which has been associated with a hexagonal warping distortion.[21] In the absence of SO coupling the two states maintain their degeneracy far away from the Γ point until they lose their surface character.

IV. SURFACE DYNAMICS

The surface phonon dispersion curves were calculated for both a 12-layer and a 24-layer slab without SO interaction, and for a 12-layer slab with the inclusion of the SO interaction. The effect of SO coupling is marginal, resulting in an overall softening of at most 1% of the optical modes. The phonon spectrum of Sb(111) consists of two bands separated by a 4-meV gap, originating from the acoustic and optical branches of bulk phonons.

The surface phonon spectrum projected onto the first surface layer in Fig. 4 is characterized by three surface-localized modes clearly separated from the bulk bands: (i) the Rayleigh wave (S1), running below the lower edge of the acoustic bulk band; (ii) a gap mode (S6) appearing in the acoustic region at 8.5 meV near the *K* point; and (iii) a surface branch (S2) localized above the maximum of the bulk continuum in the optical region. Moreover, three strong surface resonances are found in the bulk continuum associated with the longitudinal acoustic band (the longitudinal resonance S3) and the transverse optical bands (the Lucas modes S4 and S5). The frequencies of these surface phonon branches change less than 1% by increasing the slab thickness from 12 to 24 layers. The character and polarization of the surface phonon branches is evidenced by representing the longitudinal (L1, L2, L3), shear horizontal (SH1, SH2, SH3), and shear vertical (SV1, SV2, SV3) polarization components projected on the first (Fig. 4), second (Fig. 5), and third (Fig. 6) surface layer. The analysis of the polarization in Figs. 4–6 and the direct inspection of phonon eigenmodes allowed assigning the character of surface phonons as described below. The dispersion of the Rayleigh wave (S1) shows a rather unusual behavior at the zone boundary, where its quasi-SV polarization present at long wavelengths is preserved only in the second layer while it turns into a longitudinal polarization in the first layer. In approaching the zone boundary, the first layer SV polarization is transferred to the upper resonance S3, which loses its peculiar longitudinal polarization at long wavelengths. The latter resonance exhibits, however, a full L polarization in the second layer. This behavior is exactly the opposite of that observed for the longitudinal acoustic resonance in practically all metal surfaces.[22,23] Layered semimetals like Sb(111) behave differently from ordinary metals because of the partially covalent bonds between the first and second layer. The comparatively strong bonds within the first bilayer are also responsible for the appearance of the SV surface branch S2 localized above the bulk optical band. The similar intensities of SV1 and SV2 at the Γ point indicate a bilayer compressional mode. It is interesting to note that the S2 mode preserves its SV polarization in the first layer (SV1), even when merging

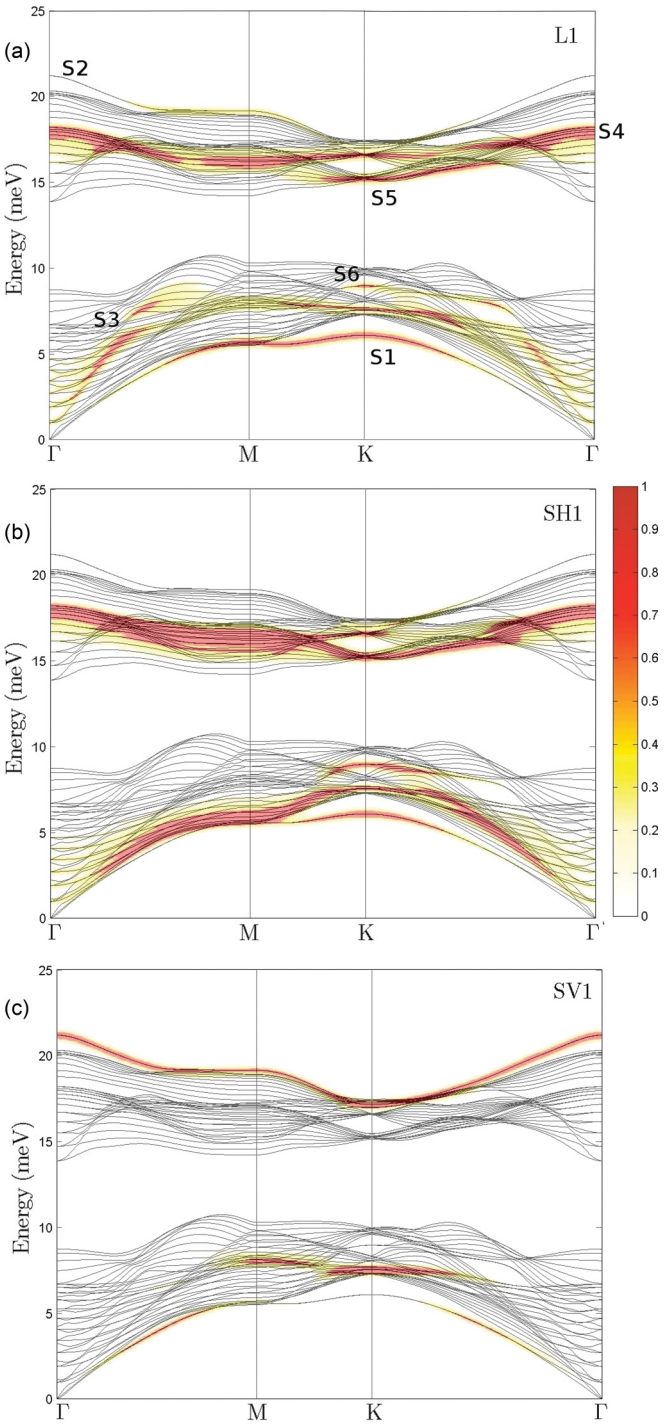

FIG. 4. (Color online) Dispersion curves of a Sb(111) 24-layer slab from a DFPT calculation without SO coupling. Highlighted branches represent surface-localized modes and resonances for (a) longitudinal (L1), (b) shear horizontal (SH1), and (c) shear vertical (SV1) polarization. Their intensity projected onto the first surface layer is given by the gray code in panel (b).

at the zone boundary into the upper edge of the optical bulk band, whereas in the second layer it acquires a longitudinal polarization (L2). Similarly to the S2 mode, the two Lucas

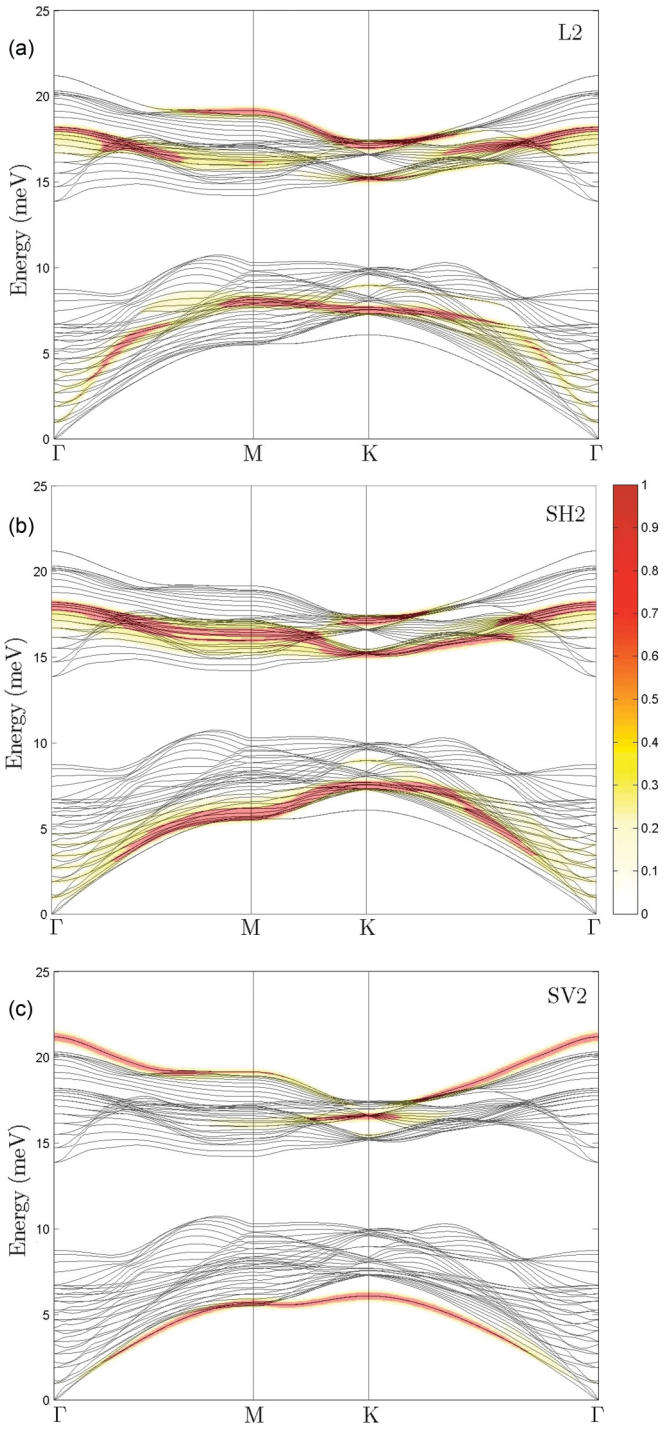

FIG. 5. (Color online) Dispersion curves of a Sb(111) 24-layer slab from a DFPT calculation without SO coupling. Highlighted branches represent surface-localized modes and resonances for (a) longitudinal (L2), (b) shear horizontal (SH2), and (c) shear vertical (SV2) polarization. Their intensity projected onto the second surface layer is given by the gray code in panel (b).

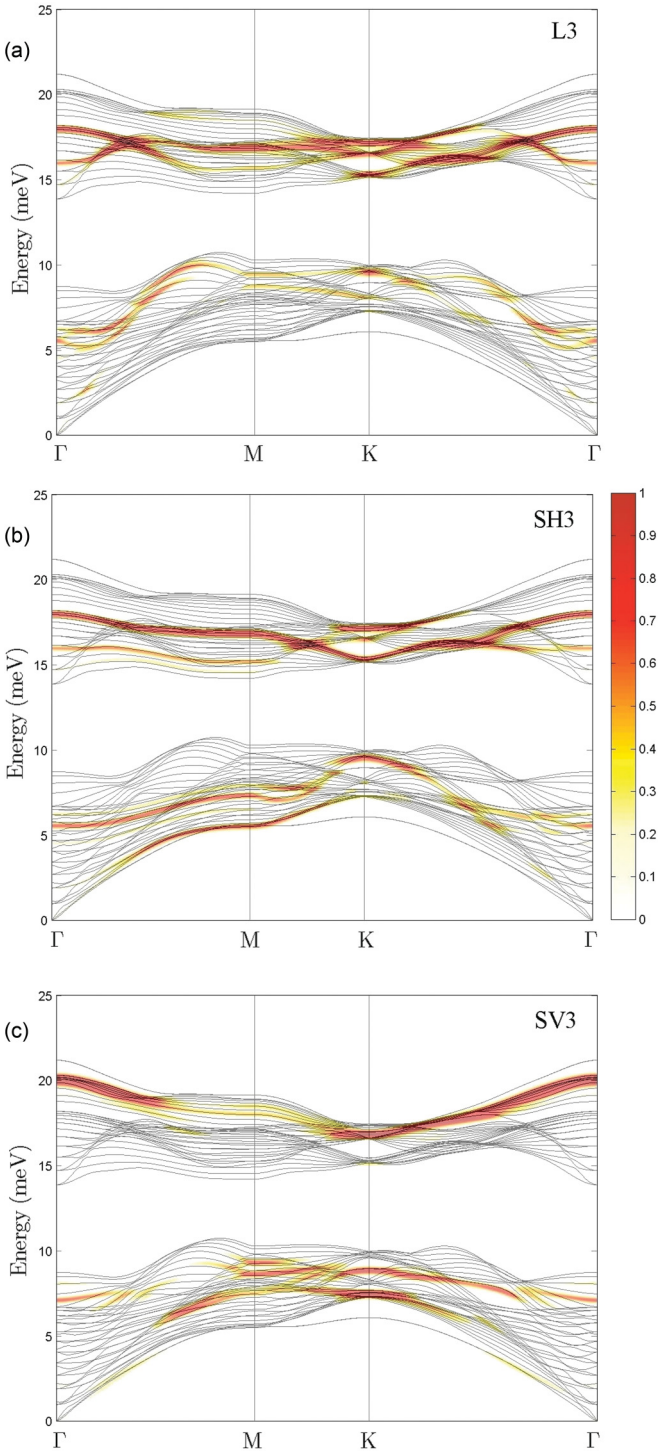

FIG. 6. (Color online) Dispersion curves of a Sb(111) 24-layer slab from a DFPT calculation without SO coupling. Highlighted branches represent surface-localized modes and resonances for (a) longitudinal (L3), (b) shear horizontal (SH3), and (c) shear vertical (SV3) polarization. Their intensity projected onto the third surface layer is given by the gray code in panel (b).

mode broad resonances (degenerate at Γ) correspond to an out-of-phase displacement of the two surface layers within the surface plane, either longitudinal (S4) or transverse (S5). In the acoustic region there is a gap mode around the *K* point at about 8 meV. This mode is the final part of a shear vertical resonance, mainly localized on the third layer (cf. Fig. 6), that crosses all the SBZ and originates at the Γ point with an energy of 7 meV. The occurrence of phonon resonances with a prominent localization on the third atomic layer (actually the second bilayer) (cf. Fig. 6) is due to the fact that the intrabilayer

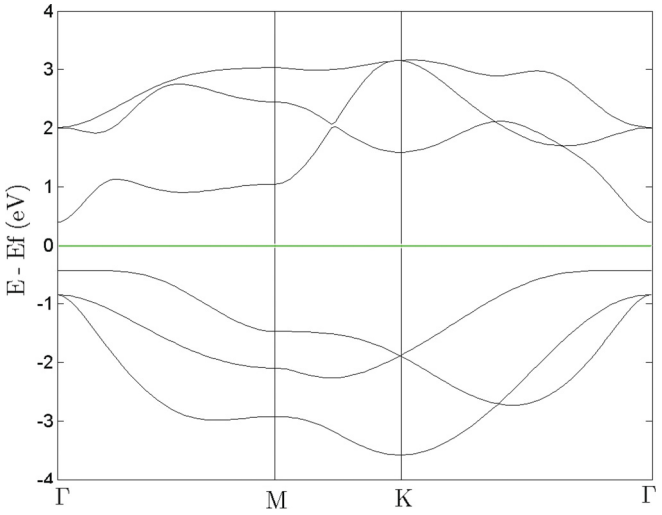

FIG. 7. (Color online) Electronic bands of a single Sb(111) bilayer.

force constants are considerably stronger than the interbilayer force constants.

The surface optical mode above the topmost edge of the bulk is also present in the phonons of a single bilayer. The bilayer of Sb is semiconducting with a band gap of 0.8 eV (cf. Fig. 7) and we verified that it is a normal insulator, i.e., its Z_2 (Ref. 24) topological index is zero. The in-plane lattice parameter was fixed to the bulk value. The distance between the two layers increases by 0.9%. The phonon dispersion relations of the Sb bilayer are reported in Fig. 8, where the color indicates the contributions from different polarizations (L, SH, SV). This calculation shows that the Sb bilayer is stable and that the highest phonon energy band is higher in energy than the corresponding band of the Sb(111) surface.

V. ELECTRON-PHONON INTERACTION

Electron-phonon interaction is responsible for the linewidth of surface electronic states obtained, for instance, by angle-resolved photoemission measurement.[3] The experimental analysis of the linewidth of photoemission peaks from the topologically nontrivial surface states in Ref. 3 assigned an effective electron-phonon coupling constant λ of 0.22 ± 0.03. This was obtained by expressing the photoemission peak linewidth of a surface state at the Fermi level as $\Gamma_{\mathrm{el-ph}}(\vec{k}) = 2\pi\lambda(\vec{k})k_BT$ for a temperature T much higher than the Debye temperature. We computed the value of $\lambda(\vec{k})$ averaged over the Fermi surface for the surface bands as

$$\bar{\lambda} = \langle\lambda(\vec{k})\rangle_{E_F} = 2\int_0^\infty \frac{\alpha^2F(\omega)}{\omega}d\omega, \tag{1}$$

where E_F is Fermi energy, and $\alpha^2F(\omega)$ is the Eliashberg spectral function, which measures the contribution of phonons with frequency ω to the electron-phonon coupling:

$$\alpha^2F(\omega) = \frac{1}{N(E_F)}\sum_{\vec{q},\nu}\delta(\omega-\omega_{\vec{q},\nu}) \times \sum_{\vec{k},n,m}\delta(\epsilon_{\vec{k},n}-E_F)\,|\,g^{n,m}(\vec{k}\vec{q}\nu)\,|^2\,\delta(\epsilon_{\vec{k}+\vec{q},m}-E_F), \tag{2}$$

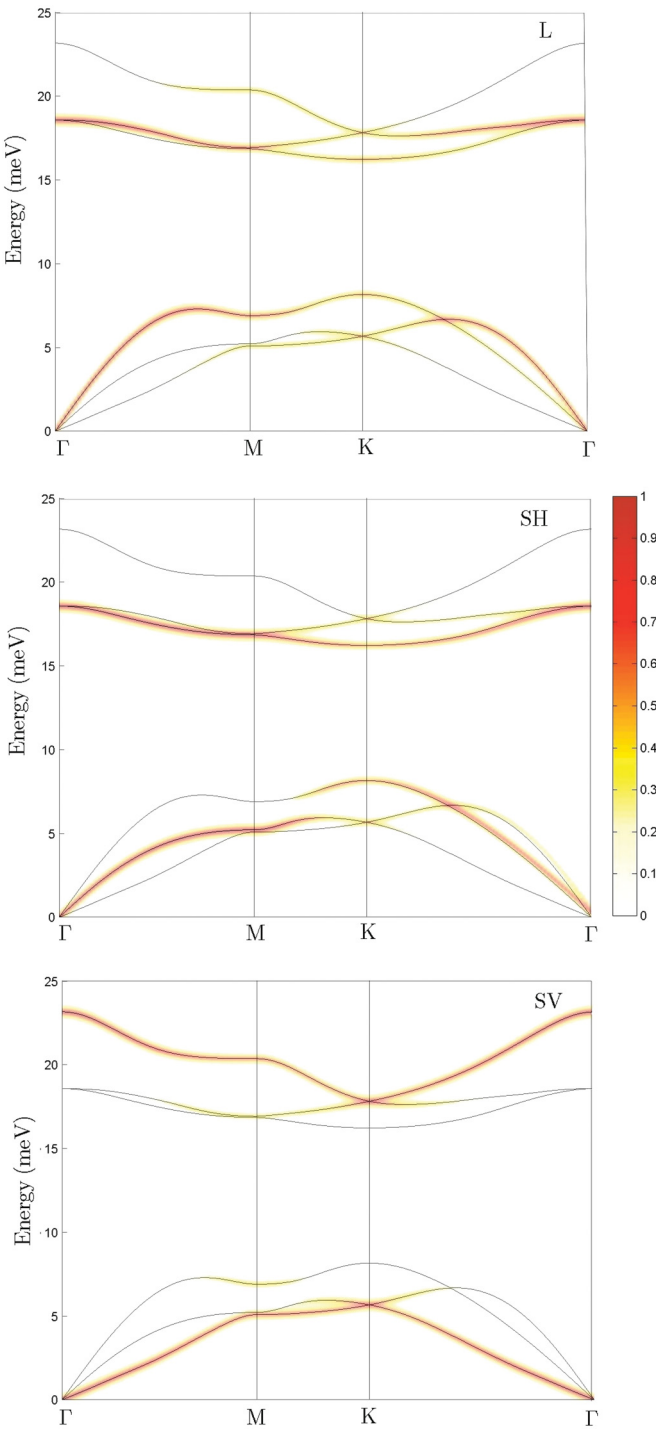

FIG. 8. (Color online) Phonon dispersions for a single Sb(111) bilayer. The gray code reported in the central panel indicates the contributions from different polarizations.

where $g^{n,m}(\vec{k}\vec{q}\nu)$ is the electron-phonon matrix element, $\epsilon_{\vec{k},n}$ and $\epsilon_{\vec{k}+\vec{q},m}$ are electronic energies, and $N(E_F)$ is the electronic density of states at the Fermi energy. The first sum runs over phonon modes, while in the second sum the index n runs over surface electronic states and the index m over surface and bulk electronic states. The two δ functions containing the electron band energies were replaced by an order one Hermite-Gauss

smearing function with different values of variance ranging from 0.005 to 0.05 Ry.[25] As stated in Ref. 26, most of the variations of the value of λ with the size of k- and q-point meshes can be ascribed to fluctuations in the density of states at the Fermi level. To achieve a faster convergence with respect to $\vec{q}$ and $\vec{k}$ sums we calculated a quantity normalized with respect to the density of states $\alpha^2F(\omega)/N_a(E_F)$ given by

$$\frac{\alpha^2F(\omega)}{N_a(E_F)} = \frac{1}{N_a(E_F)}\frac{1}{N_s(E_F)}\sum_{\vec{q},\nu}\delta(\omega-\omega_{\vec{q},\nu}) \times \sum_{\vec{k},n,m}\delta(\epsilon_{\vec{k},n}-E_F)\,|\,g^{n,m}(\vec{k}\vec{q}\nu)\,|^2\,\delta(\epsilon_{\vec{k}+\vec{q},m}-E_F), \tag{3}$$

where $N_s(E_F)$ is the density of states at the Fermi level for the starting states (i.e., the surface states only), while $N_a(E_F)$ is the density of states at the Fermi level for all the possible arrival states (bulk and surface ones). Then the value of λ is obtained by multiplying by a more accurate value of $N_a(E_F)$ computed using the tetrahedron method over a uniform $60\times60\times1$ k-point mesh. We estimated a total error in λ below 10%. The electron-phonon matrix elements are computed by means of DFPT on a dense $40\times40\times1$ k-point grid and a $60\times60\times1$ q-point grid for a 12-layer slab without SO coupling. We remark that λ in Eqs. (1)–(3) involves only processes due to electrons in surface states that can jump into another surface state or into a bulklike state at the Fermi level. For the sake of comparison we computed the electron-phonon coupling constant in the bulk, obtaining $\lambda_B = 0.17$. The value of λ_B is obtained with $60\times60\times60$ and $60\times60\times60$ k and q meshes. To the best of our knowledge there are no experimental data or previous DFT calculations to compare with this result for λ_B. The phonon density of states $F(\omega)$ and the Eliashberg function $\alpha^2F(\omega)$ for the bulk and the surface are reported in Fig. 9. The surface phonon density of states is obtained by projecting on the atoms of the surface bilayer only. The $\alpha^2F(\omega)$ function of the surface is very similar to that of the bulk. The most noticeable difference is a more pronounced peak at around 6 meV due to the contribution of the Rayleigh wave that, however, contributes far less than 10% to the value of λ. The resulting $\lambda = 0.27$ is mostly the result of the transition of the surface electrons into bulk states at the Fermi level as driven by bulk phonons. The fact that bulk phonons mostly contribute to the linewidth of the surface electronic states at E_F was actually proposed in Ref. 3 from the analysis of the linewidth of the electronic states as a function of energy below E_F measured by ARPES. By fitting the dependence of the linewidth on energy with both surface and bulk Debye models with the Debye energy and λ as free parameters, an anomalously high value of λ was found with the surface model, while the bulk model produced a value of λ close to that (0.22) measured from the temperature dependence of the linewidth at E_F. By neglecting transitions into bulklike and thus including only intraband transitions of the surface states, the electron-phonon coupling constant drops to values below 0.01. We remark that the calculation of λ was carried out without including SO coupling, which is expected to reduce further the contribution to λ from intraband transition among the surface electronic states. Since the latter is already very small (0.01), the contribution of SO coupling to λ is expected to be negligible.

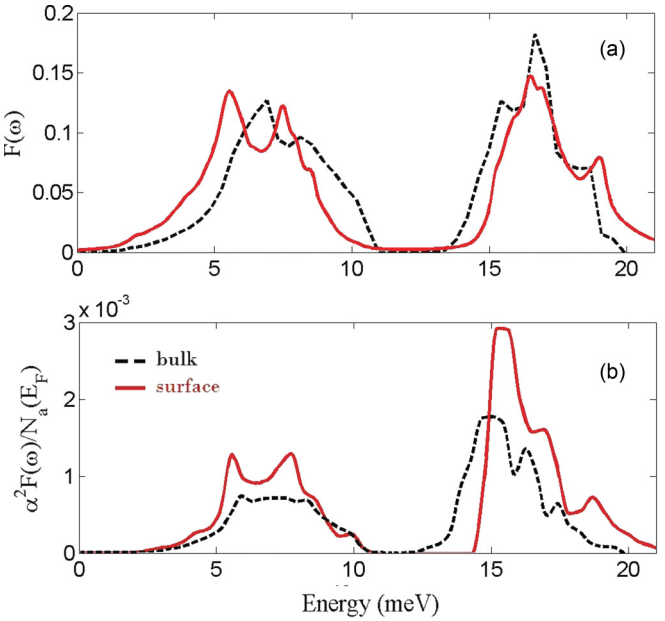

FIG. 9. (Color online) (a) Surface-projected phonon density of states of Sb(111) (solid line) compared to the phonon density of states for bulk Sb (dashed line). The normalized Eliashberg functions for the bulk and the surface electronic states are shown in panel (b).

VI. CONCLUSIONS

Although Sb crystals belong to the wide class of layered structures, with a weak inter-bilayer interaction, the surface bilayer turns out to be considerably stiffer than the deeper layers in the bulk. This behavior results in remarkable dynamic features, such as the appearance of a strongly localized SV phonon branch above the bulk maximum and the conversion of the Rayleigh branch into a surface longitudinal mode at the zone boundary. Moreover, the self-standing single bilayer is found to be stable, with an optical phonon branch stiffer than the corresponding bulk branch. The second-bilayer resonances in the acoustic region, starting at Γ, at approximately 6 meV for L3 and SH3 and at 7.5 meV for SV3, are analogous to Sezawa waves, known in seismology to occur at the interface of a surface layer with a substrate of different acoustic impedance (in this case the surface bilayer above the bulk lattice).[27] In a layered structure with a substantial electron-phonon interaction, deep resonances of this kind with either SV or L polarization are likely to be observable with helium atom scattering, as recently shown for subsurface phonon branches of lead overlayers.[28] The spin-orbit coupling has little effect on bulk and surface phonons. The main contribution to electron-phonon interaction involves transitions between surface and bulk states mostly driven by bulk phonons, and is found to be in good agreement with the value derived from angle-resolved photoemission spectroscopy. The phonon structure of Sb(111) could provide some hints for the analysis of the dispersion curves which are being measured in Bi(111) (Ref. 4 and papers to appear). A calculation of the six phonon branches

of the Bi(111) bilayer yields a phonon structure very similar to that of the Sb(111) bilayer (Fig. 8). Such a similarity is expected to be found also for the thick slabs, i.e., for the surface phonon structure. It is hoped that a study of Sb(111) dispersion curves by means of HAS spectroscopy will be accomplished soon.

ACKNOWLEDGMENTS

One of us (G.B.) acknowledges the support of Ikerbasque (Project ABSIDES) and useful discussions with V. Chis, E. V. Chulkov, and P. M. Echenique (DIPC, Donostia/San Sebastián).

*Corresponding author: giorgio.benedek@mater.unimib.it

[1] D. Hsieh, Y. Xia, L. Wray, D. Qian, A. Pal, J. H. Dil, J. Osterwalder, F. Meier, G. Bihlmayer, C. L. Kane, Y. S. Hor, R. J. Cava, and M. Z. Hasan, Science **323**, 919 (2009).

[2] D. Hsieh, L. Wray, D. Qian, Y. Xia, J. H. Dil, F. Meier, L. Patthey, J. Osterwalder, G. Bihlmayer, Y. S. Hor, R. J. Cava, and M. Z. Hasan, New J. Phys. **12**, 125001 (2010).

[3] K. Sugawara, T. Sato, S. Souma, T. Takahashi, M. Arai, and T. Sasaki, Phys. Rev. Lett. **96**, 046411 (2006).

[4] A. Tamtogl, M. Mayrhofer-Reinhartshuber, N. Balak, W. E. Ernst, and K. H. Rieder, J. Phys.: Condens. Matter **22**, 304019 (2010).

[5] S. Baroni, S. de Gironcoli, and A. Dal Corso, Rev. Mod. Phys. **73**, 515 (2001).

[6] P. Giannozzi, S. Baroni, N. Bonini, M. Calandra, R. Car, C. Cavazzoni, D. Ceresoli, G. L. Chiarotti, M. Cococcioni, I. Dabo, A. Dal Corso, S. de Gironcoli, S. Fabris, G. Fratesi, R. Gebauer, U. Gerstmann, C. Gougoussis, A. Kokalj, M. Lazzeri, L. Martin-Samos, N. Marzari, F. Mauri, R. Mazzarello, S. Paolini, A. Pasquarello, L. Paulatto, C. Sbraccia, S. Scandolo, G. Sclauzero, A. P. Seitsonen, A. Smogunov, P. Umari, and R. M. Wentzcovitch, J. Phys.: Condens. Matter **21**, 395502 (2009).

[7] J. P. Perdew, K. Burke, and M. Ernzerhof, Phys. Rev. Lett. **77**, 3865 (1996).

[8] L. Nordstrom and D. J. Singh, Phys. Rev. Lett. **76**, 4420 (1996).

[9] C. S. Barrett, P. Cucka, and K. Haefner, Acta Crystallogr. **16**, 451 (1963).

[10] K. Shportko, S. Kremers, M. Woda, D. Lencer, J. Robertson, and M. Wuttig, Nature Mater. **7**, 653 (2008).

[11] H. Monkhorst and J. D. Pack, Phys. Rev. B **13**, 5188 (1976).

[12] X. Wang, K. Kunc, I. Loa, U. Schwarz, and K. Syassen, Phys. Rev. B **74**, 134305 (2006).

[13] R. I. Sharp and E. Warming, J. Phys. F: Met. Phys. **1**, 570 (1971).

[14] J. Serrano, R. K. Kremer, M. Cardona, G. Siegle, L. E. Díaz-Sánchez, and A. H. Romero, Phys. Rev. B **77**, 054303 (2008).

[15] J. Serrano and A. H. Romero, High Press. Res. **28**, 477 (2008).

[16] S. Grimme, J. Antony, S. Ehrlich, and H. Kreig, J. Chem. Phys. **132**, 154104 (2010).

[17] A. D. Becke, Phys. Rev. A **38**, 3098 (1988).

[18] C. T. Lee, W. T. Yang, and R. G. Parr, Phys. Rev. B **37**, 785 (1988).

[19] G. Bian, T. Miller, and T.-C. Chiang, Phys. Rev. Lett. **107**, 036802 (2011).

[20] O. V. Yazyev, J. E. Moore, and S. G. Louie, Phys. Rev. Lett. **105**, 266806 (2010).

[21] L. Fu, Phys. Rev. Lett. **103**, 266801 (2009).

[22] V. Chis, B. Hellsing, G. Benedek, M. Bernasconi, E. V. Chulkov, and J. P. Toennies, Phys. Rev. Lett. **101**, 206102 (2008).

[23] G. Benedek, M. Bernasconi, V. Chis, E. V. Chulkov, P. M. Echenique, B. Hellsing, and J. P. Toennies, J. Phys.: Condens. Matter **22**, 084020 (2010).

[24] L. Fu and C. L. Kane, Phys. Rev. B **76**, 045302 (2007).

[25] M. Methfessel and A. T. Paxton, Phys. Rev. B **40**, 3616 (1989).

[26] I. Spagnolatti, M. Bernasconi, and G. Benedek, Europhys. Lett. **59**, 572 (2002).

[27] K. Sezawa, Bull. Earthq. Res. Inst., Tokyo Imp. Univ. **9**, 115 (1931).

[28] I. Yu. Sklyadneva, G. Benedek, E. V. Chulkov, P. M. Echenique, R. Heid, K. P. Bohnen, and J. P. Toennies, Phys. Rev. Lett. **107**, 095502 (2011).